The α6β4 integrin promotes resistance to ferroptosis

Caitlin W. Brown, John J. Amante, Hira Lal Goel, and Arthur M. Mercurio

Department of Molecular, Cell and Cancer Biology, University of Massachusetts Medical School, Worcester, MA

Increases in lipid peroxidation can cause ferroptosis, a form of cell death triggered by inhibition of glutathione peroxidase 4 (GPX4), which catalyzes the reduction of lipid peroxides and is a target of ferroptosis inducers, such as erastin. The α6β4 integrin protects adherent epithelial and carcinoma cells from ferroptosis induced by erastin. In addition, extracellular matrix (ECM) detachment is a physiologic trigger of ferroptosis, which is evaded by α6β4. The mechanism that enables α6β4 to evade ferroptosis involves its ability to protect changes in membrane lipids that are proferroptotic. Specifically, α6β4-mediated activation of Src and STAT3 suppresses expression of ACSL4, an enzyme that enriches membranes with long polyunsaturated fatty acids and is required for ferroptosis. Adherent cells lacking α6β4 require an inducer, such as erastin, to undergo ferroptosis because they sustain GPX4 expression, despite their increase in ACSL4. In contrast, ECM detachment of cells lacking α6β4 is sufficient to trigger ferroptosis because GPX4 is suppressed. This causal link between α6β4 and ferroptosis has implications for cancer biology and therapy.

Introduction

The ability of cells to resist death is a hallmark of tissue homeostasis and disease, especially cancer (Hanahan and Weinberg, 2011). With respect to cancer, resistance to chemotherapy-induced cell death is a problem of paramount importance (Safa, 2016). In addition, adverse conditions in the tumor microenvironment, such as detachments from matrix (anoikis), result in cell death, and tumor cells must acquire mechanisms to resist such death to survive and progress to metastatic disease (Buchheit et al., 2014). Our interest in this area has been awakened by the discovery of a novel mode of programmed cell death, termed ferroptosis. Ferroptosis is defined as an iron-dependent form of programmed cell death, which is characterized by lipid reactive oxygen species (ROS) accumulation that damages the plasma membrane by peroxidation of polyunsaturated fatty acids (Yang et al., 2016; Yang and Stockwell, 2016). At a mechanistic level, ferroptosis is triggered by the loss of activity for the lipid repair enzyme glutathione peroxidase 4 (GPX4), which catalyzes the reduction of lipid and other peroxides and is a target of several ferroptosis inducers (Yang et al., 2014). The antiporter system X_C^-, which imports cystine into the cell in exchange for glutamate, also has a critical role in protecting against ferroptosis because cysteine, the monomeric form of cystine, is converted to the antioxidant glutathione, which is a substrate for GPX4 (Yang and Stockwell, 2016). Molecules that inhibit system X_C^-, such as erastin, trigger ferroptosis, and they have proven to be useful for studying this process in detail (Dixon et al., 2012).

At present, the significance of ferroptosis in the context of epithelial and carcinoma biology is still emerging. The findings that ferroptosis inducers can inhibit the growth of tumor xenografts have heightened the cancer relevance of this mode of cell death (Yang et al., 2014; Kim et al., 2016). Although exciting, these findings do not provide insight into the mechanisms used by cells to evade ferroptosis or whether tumor cells encounter conditions that trigger ferroptosis and, consequently, whether they must acquire mechanisms to evade this process. The study that reported that p53-mediated tumor suppression involves ferroptosis (Jiang et al., 2015) provided some indication of the physiological relevance of this process in cancer. Ferroptosis also occurs in p53 mutant cells (Jiang et al., 2015) indicating that mechanisms other than loss of p53 function are involved in promoting resistance to ferroptosis.

Given the existing literature, we were intrigued by the possibility that integrin signaling protects cells from ferroptosis. We were particularly interested in the integrin α6β4 because several seminal studies have revealed that this integrin can protect epithelial and carcinoma cells from death in adverse conditions (Lipscomb and Mercurio, 2005; Giancotti, 2007), and it has been implicated in metastasis. In this study, we uncovered a key role for α6β4 in the evasion of ferroptosis, and we pursued the mechanisms involved.

Results

The integrin α6β4 promotes resistance to erastin-induced ferroptosis

Initially, we assessed the susceptibility of MCF-10A (immortalized breast epithelial cells) and SUM-159 (breast carcinoma

Correspondence to Arthur M. Mercurio: arthur.mercurio@umassmed.edu

Abbreviations used: DFO, deferoxamine; DPP, 5,15-diphenylporphyrin; GPX4, glutathione peroxidase 4; LDH, lactate dehydrogenase; MDA, malondialdehyde; PAM, protospacer-adjacent motif; PDX, patient-derived xenograft; polyHEMA, 2-hydroxyethyl methacrylate; qPCR, quantitative PCR; ROS, reactive oxygen species; Z-VAD-FMK, carbobenzoxy-valyl-alanyl-aspartyl-[*O*-methyl]-fluoromethylketone.

The Rockefeller University Press
J. Cell Biol. Vol. 216 No. 12 4287–4297
https://doi.org/10.1083/jcb.201701136

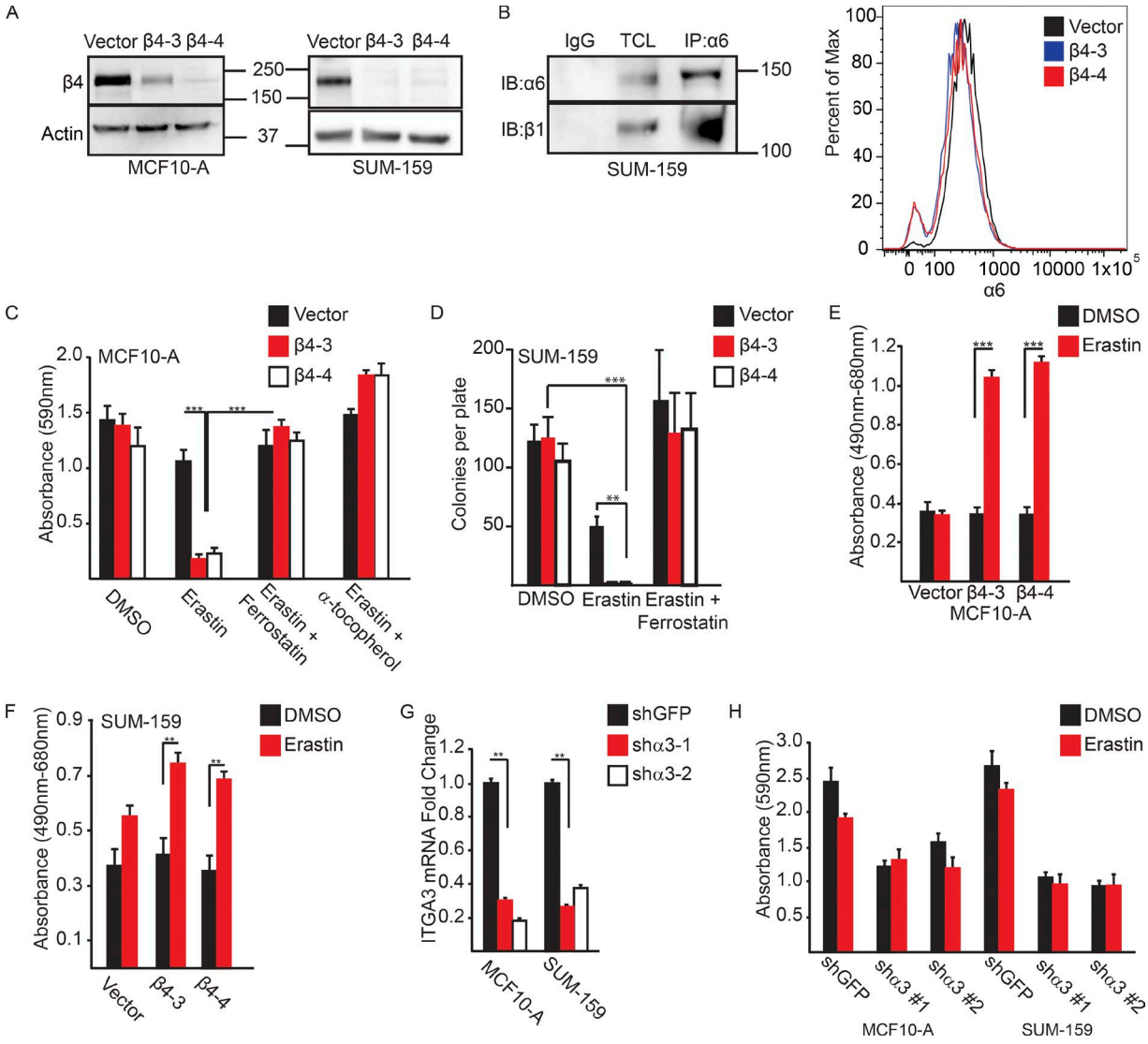

Figure 1. **The α6β4 integrin promotes evasion of ferroptosis induced by erastin.** (A) The β4-integrin subunit was depleted in MCF10-A and SUM-159 cells by CRISPR/CAS9 using two independent guide RNAs (β4-3 and β4-4). Depletion of β4 expression was verified by immunoblotting. (B) Extracts of β4-depleted cells were immunoprecipitated with an α6 antibody and immunoblotted with a β1 antibody to verify that these cells express α6β1 (left blot). Vector control and β4-depleted cells were assessed for surface expression of the α6-integrin by flow cytometry. (C and D) Control and β4-depleted MCF10-A or SUM-159 cells (5×10^2) were plated in 60-mm dishes in the presence of either DMSO, 10 µM erastin, erastin and 2 µM ferrostatin-1, or erastin and 500 µM α-tocopherol, and survival was quantified after 7 d by either DMSO extraction of crystal violet-stained cells or colony counting, respectively. (E and F) MCF10-A or SUM-159 vector control and β4-depleted cells were assayed for LDH after 6 h of treatment with either DMSO control or 10 µM erastin. (G) shRNA-mediated depletion of the α3-integrin subunit in MCF10-A and SUM-159 cells was confirmed by qPCR after 7 d of puromycin selection. (H) MCF10-A and SUM-159 α3-depleted cells were plated at clonal density, and survival was quantified as in C and E. All experiments were performed independently three times, and a representative experiment is shown. The bars in graphs represent means ± SD. *, $P < 0.05$; **, $P < 0.01$; ***, $P < 0.005$.

cells) to undergo cell death after treatment with erastin, a ferroptosis inducer (Dixon et al., 2012) as a function of α6β4 expression. For that purpose, we generated a CRISPR/Cas9 deletion of the β4 subunit of the α6β4 heterodimer (Fig. 1 A), leaving the α6β1 heterodimer intact, as assessed by immunoblotting and flow cytometry (Fig. 1 B). We observed that MCF-10A cells that lacked α6β4 were significantly less viable in the presence of erastin compared with control cells, as assessed by colony formation assays (Fig. 1 C). The loss of viability in α6β4-depleted cells in response to erastin was rescued by the addition of ferrostatin-1, a specific inhibitor of ferroptosis (Dixon et al., 2012), or by the addition of lipophilic antioxidant α-tocopherol (Fig. 1 C). Similar results were obtained with SUM-159 cells (Fig. 1 D). Given that ferroptosis is a form of programmed necrosis (Dixon et al., 2012), we used the lactate dehydrogenase (LDH) assay to assess cytotoxicity in response to erastin. Treatment of α6β4-depleted MCF-10A cells (Fig. 1 E) or SUM-159 cells (Fig. 1 F) with erastin significantly increased extracellular LDH activity, which was not observed with control cells.

An important issue is whether the ability of α6β4 to evade erastin-induced ferroptosis is specific to this integrin. As shown in Fig. 1 B, α6β4-depleted cells expressed the α6β1 integrin, but that integrin was not sufficient to evade ferroptosis under those conditions. We also targeted the α3β1 integrin because it is a laminin receptor expressed by epithelial and carcinoma cells (DiPersio et al., 1997). Expression of the α3 subunit was diminished in both MCF-10A and SUM-159 cells

using shRNAs, and α3 mRNA expression was evaluated by quantitative PCR (qPCR; Fig. 1 G). The α3-depleted cells, in contrast to the β4-depleted cells, were not sensitive to erastin, although they did form significantly fewer colonies than control cells did (Fig. 1 H).

ECM detachment triggers ferroptosis: Evasion by α6β4

The ability of the integrin α6β4 to protect against erastin-induced ferroptosis has important implications for drug targeting. Nonetheless, little is known about pathophysiological stimuli that trigger ferroptosis. Based on previous work indicating that α6β4 can promote cell survival in stress conditions (Bachelder et al., 1999; Zahir et al., 2003), we assessed the susceptibility of α6β4-depleted cells to ferroptosis after detachment from the ECM. We observed that ECM-detached MCF-10A and SUM-159 cells lacking α6β4, but not control cells, exhibited a substantial decrease in viability after 24 h (Fig. 2 A). Ferrostatin-1 treatment of α6β4-depleted cells resulted in a partial rescue of the viability of matrix-detached cells (Fig. 2 A). Similar results were obtained with Hs578t cells, another breast cancer cell line (Fig. 2 B). Treatment with other ferroptosis inhibitors, including liproxstatin-1 (Fig. 2 C; Friedmann Angeli et al., 2014), the iron chelator deferoxamine (DFO), trolox, and α-tocopherol (Dixon et al., 2012), also resulted in a partial rescue of cell death caused by matrix detachment and loss of α6β4 (Fig. 2 D). Detachment of α6β4-depleted cells increased cytotoxicity significantly compared with control cells, as assessed by the LDH assay, and that increase was prevented by ferrostatin-1 (Fig. 2 E).

We also assayed cell viability as a function of time in the presence of ferrostatin-1 using control and α6β4-depleted cells (Fig. 2 F). That analysis revealed that ferroptosis occurs rapidly in the absence of α6β4 (between 4 and 12 h), which is consistent with the LDH data on adherent cells treated with erastin (Fig. 1, E and F). Because anoikis has been studied primarily as a form of apoptosis (Meredith et al., 1993; Frisch and Francis, 1994), we compared the ability of carbobenzoxy-valyl-alanyl-aspartyl-[*O*-methyl]-fluoromethylketone (Z-VAD-FMK) and ferrostatin-1 to rescue the viability of α6β4-depleted cells after ECM detachment. Each of those inhibitors individually was able to affect a partial rescue, and the combination of both inhibitors rescued viability completely (Fig. 2 G).

To control for the specificity of α6β4 depletion, we engineered a β4 expression construct that could not be targeted by CRISPR–Cas9. Expression of that construct in α6β4-depleted cells protected those cells from the loss of viability caused by ECM detachment (Fig. 3 A). We also assessed the viability of the MCF10-A and SUM-159 α3-depleted cells used in Fig. 1 G in detached conditions and found a moderate decrease in viability that was not rescued with ferrostatin-1 (Fig. 3 B).

We extended our analysis of ferroptosis induced by ECM detachment to human breast tumors. For that purpose, we used patient-derived xenografts (PDXs) of triple-negative breast tumors. After isolation, dissociation, and lineage depletion, tumor cells were sorted based on the level of β4 surface expression into $\beta4^{high}$ and $\beta4^{low}$ populations, taking the top and bottom quartiles, respectively (Fig. 3 C). Those two populations were assessed for viability in detached conditions, either in the presence or absence of ferrostatin-1. Under those conditions, the $\beta4^{low}$ population was significantly less viable than the $\beta4^{high}$ population, and that loss of viability was rescued by ferrostatin-1 (Fig. 3 D).

Src, which is activated by α6β4, protects against ferroptosis

The signaling pathways that enable cells to evade ferroptosis are poorly understood. We focused on the potential role of Src, because several studies have documented the robust activation of Src by α6β4, and examined the functional consequences (Gagnoux-Palacios et al., 2003; Bertotti et al., 2006; Merdek et al., 2007; Dutta and Shaw, 2008; Yang et al., 2010; Sharma et al., 2012; Pavlova et al., 2013; Hoshino et al., 2015). Activation of Src in α6β4-depleted MCF-10A and SUM-159 cells was significantly reduced compared with vector controls, as assessed by Y418 immunoblotting (Fig. 4 A), indicating that α6β4 promotes Src activation in ECM detachment. To evaluate a causal role for Src activation in ferroptosis evasion, control cells were treated with the Src inhibitor PP2 and assayed for viability 24 h after detachment (Fig. 4 B). Strikingly, Src inhibition decreased cell viability significantly, and that loss of viability was rescued by ferrostatin-1 and other ferroptosis inhibitors (Fig. 4 B).

Next, we assessed Src activation in adherent cells in response to erastin based on the assumption that erastin treatment stresses cells and elicits a response to diminish that stress. Indeed, erastin treatment of control MCF-10A and SUM-159 cells significantly increased Src activation compared with α6β4-depleted cells (Fig. 4 C). Moreover, the viability of detached, α6β4-depleted cells was rescued by expression of an inducible, constitutively active Src (Fig. 4 D). These findings support the hypothesis that α6β4 facilitates Src activation in response to stress (ECM detachment or inhibition of the system X_C^- by erastin).

In pursuit of the mechanism by which Src activation protects against ferroptosis, we were intrigued by the recent studies that found the enzyme acyl-CoA synthetase long-chain family member 4 (ACSL4) is required for ferroptosis because it synthesizes polyunsaturated fatty acids that are the primary target of lipid peroxidation (Doll et al., 2017). We quantified *ACSL4* mRNA expression in MCF10-A and SUM-159 control and α6β4-depleted cells in adherent and detached conditions (Fig. 5 A) and found a significant elevation of *ACSL4* mRNA with the loss of α6β4 in both conditions. This elevation of ACSL4 expression was also seen at the protein level in α6β4-depleted cells (Fig. 5 B). Src inhibition increased *ACSL4* expression in control cells (Fig. 5 C), indicating that it has a causal role in regulating this key ferroptotic enzyme. Moreover, reexpression of the β4 subunit in α6β4-depleted cells repressed *ACSL4* (Fig. 5 D), confirming that the repression of *ACSL4* expression is specific to α6β4-mediated signaling. Inhibition of ACSL4 using the thiazolidinedione rosiglitazone (Askari et al., 2007; Doll et al., 2017) increased the viability of detached, α6β4-depleted cells, confirming the key role of ACSL4 in ferroptosis susceptibility (Fig. 5 E). In addition, expression of constitutively active Src suppressed the expression of ACSL4 (Fig. 5 F). These in vitro data were substantiated by comparing β4 and ACSL4 expression in a cohort of patients with breast cancer using cBioportal, where a significant inverse correlation was detected (Fig. 5 G).

The preceding data raise the issue of how α6β4-mediated Src activation represses ACSL4 expression. We focused on STAT3 because it can be activated by Src (Yu et al., 1995) and, more specifically, by the α6β4-Src signaling axis (Guo et al., 2006). Moreover, STAT3 can repress, as well as activate, transcription (Niu et al., 2005). Using the ENCODE database, we identified STAT3 binding in several regions of the *ACSL4*

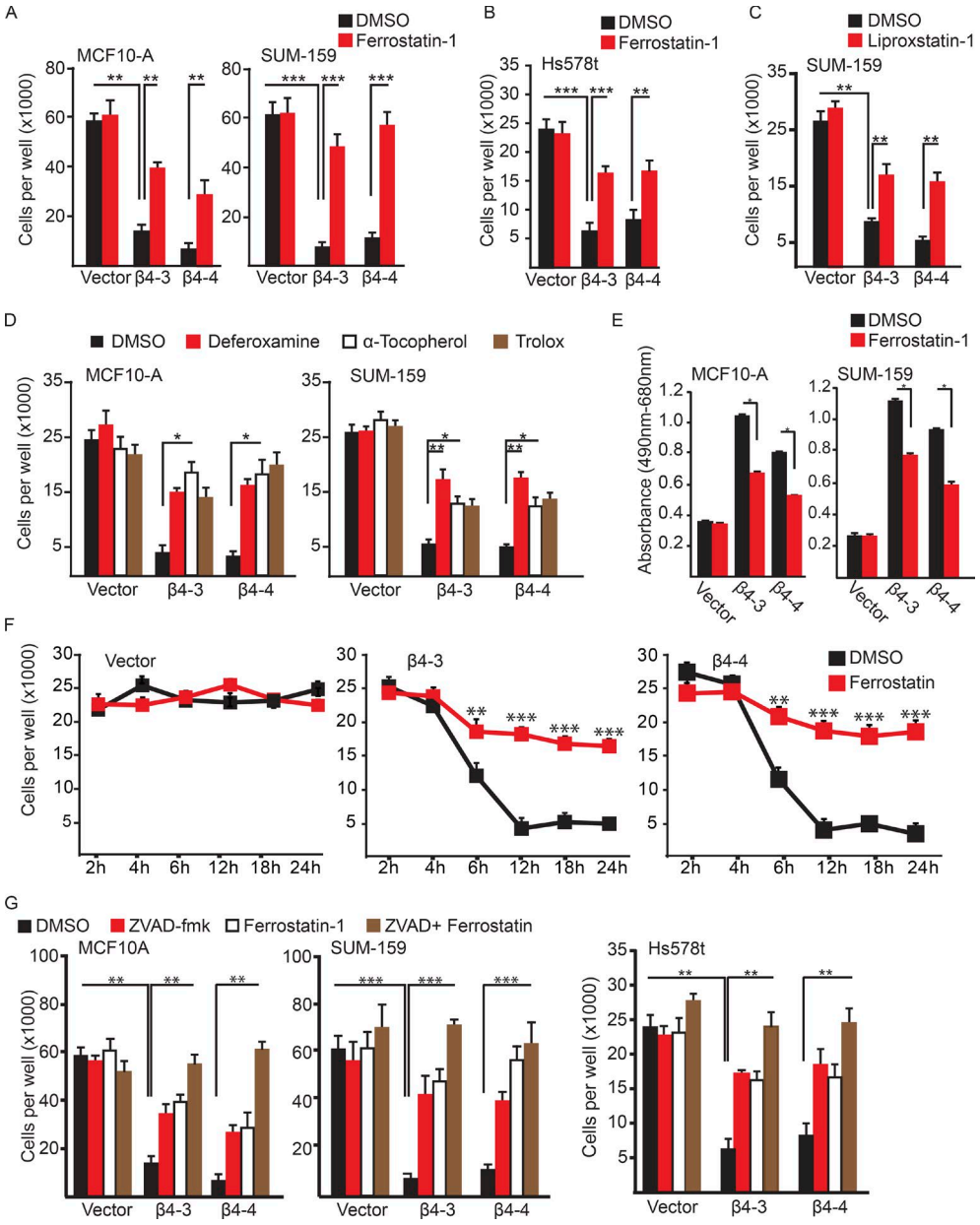

Figure 2. **Matrix-deprived cells are susceptible to ferroptosis in the absence of the α6β4-integrin.** (A) Control and β4-depleted cells were detached for 24 h in the presence of either DMSO or 2 µM ferrostatin-1, and the number of viable cells was quantified. (B) Control and β4-depleted Hs578t cells were detached for 24 h in the presence of either DMSO or 2 µM ferrostatin-1, and the number of viable cells was quantified. (C) Control and β4-depleted SUM-159 cells were detached for 24 h in the presence of either DMSO or 2 µM liproxstatin-1, and the number of viable cells was quantified. (D) Control and β4-depleted MCF-10A and SUM-159 cells were detached for 24 h in the presence of either DMSO, 100 µM DFO, 100 µM α-tocopherol, or 500 µM Trolox, and the number of viable cells was quantified. (E) MCF10-A or SUM-159 vector control and β4-depleted cells were assayed for LDH after 6 h of detachment with either DMSO or 2 µM ferrostatin-1. (F) Vector and β4-depleted cells were incubated for the times indicated with either DMSO or 2 µM ferrostatin-1, and viable cells were quantified. (G) Vector and β4-depleted cells were detached for 24 h in the presence of either DMSO, 2 µM ferrostatin-1, 25 µM Z-VAD-FMK, or ferrostatin-1 and Z-VAD-FMK, and the number of viable cells was quantified. All experiments were performed independently three times and a representative experiment is shown. The bars in graphs represent means ± SD. *, P < 0.05; **, P < 0.01; ***, P < 0.005.

promoter and coding regions of MCF10A cells (Fig. 6 A). We also observed that STAT3 phosphorylation was decreased in α6β4-depleted cells compared with control cells after erastin treatment (Fig. 6, B and C) and ECM detachment (Fig. 6, D and E). In addition, inhibition of STAT3 using 5,15-diphenylporphyrin (DPP) increased ACSL4 expression (Fig. 6 F). DPP had no effect on cell viability during the course of that assay (unpublished data). Collectively, these data indicate that α6β4-mediated Src–STAT3 activation represses expression of ACSL4, rendering the cell unable to undergo to ferroptosis.

ECM detachment requires an up-regulation of GPX4 to avoid ferroptosis

One question that arises from these data is why adherent, α6β4-depleted cells require erastin treatment to induce ferroptosis, whereas the same cells in ECM-detached conditions undergo ferroptosis spontaneously? As mentioned, ACSL4 is necessary, but not sufficient, for ferroptosis (Doll et al., 2017). Therefore, we sought to identify a regulator of ferroptosis that was altered in detached, but not adherent, conditions. We focused on GPX4 because of its central role in ferroptosis and

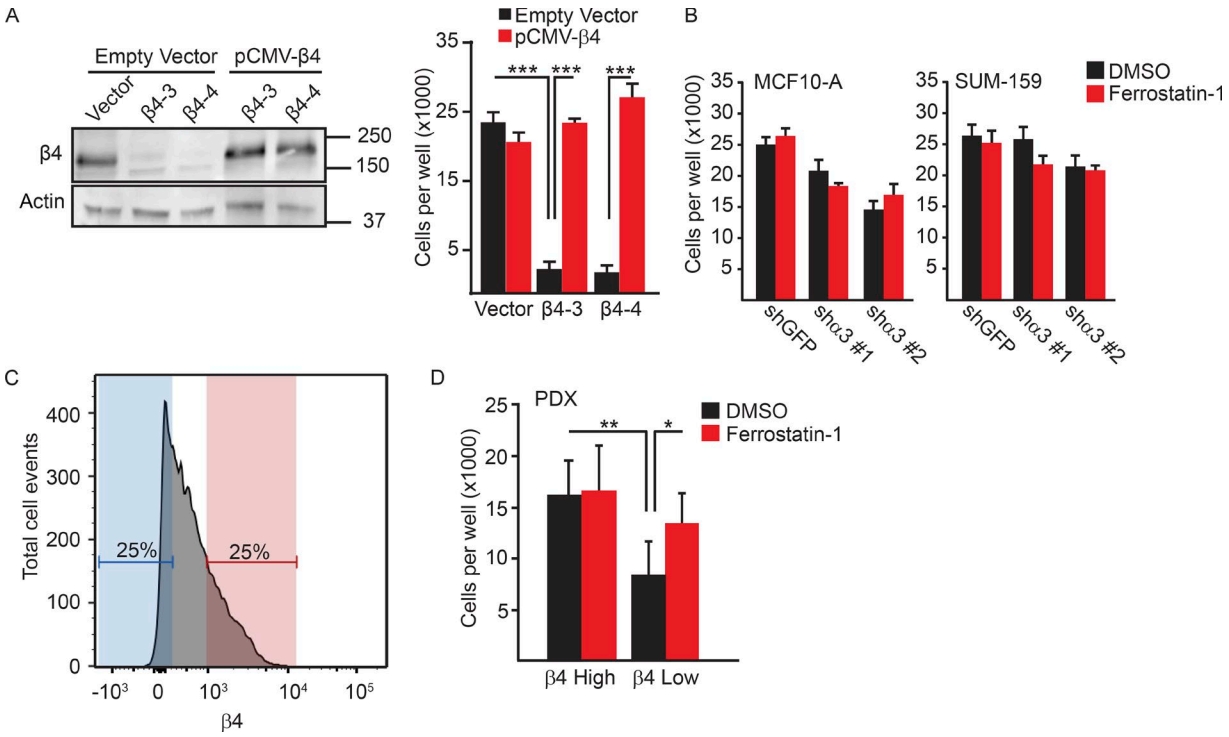

Figure 3. **Evasion of ferroptosis is specific to the α6β4-integrin.** (A) β4-depleted SUM-159 cells were transfected with either a control plasmid (vector) or a β4 expression construct in which the PAM sequences targeted by the guide RNAs were mutated. Rescue of β4 expression was confirmed by immunoblotting and qPCR. Vector control cells, β4-depleted cells, vector control cells transfected with β4 containing PAM mutations, and β4-depleted cells transfected with β4 containing PAM mutations (β4-rescued cells) were detached for 24 h, and the number of viable cells was quantified. (B) MCF10-A and SUM-159 α3-depleted cells were detached and compared with control cells for their viability after 24 h. (C and D) PDXs of triple-negative breast tumors were isolated, dissociated, and lineage-depleted, and the tumor cells were sorted based on the level of β4 surface expression into $\beta4^{high}$ (red) and $\beta4^{low}$ (blue) populations. Those two populations were assessed for viability in detached conditions, either in the presence or absence of ferrostatin-1. All experiments were performed independently three times, and a representative experiment is shown. The bars in graphs represent means ± SD. *, P < 0.05; **, P < 0.01; ***, P < 0.005.

its ability to buffer lipid peroxidation. Moreover, GPX4 is the only glutathione peroxidase that accepts phospholipid hydroperoxides in membranes as oxidizing substrates (Thomas et al., 1990; Roveri et al., 1994; Seiler et al., 2008). There was no significant difference in GPX4 expression in adherent conditions between control and α6β4-depleted cells (Fig. 7 A). However, we observed that ECM detachment caused an increase in GPX4 expression and that cells lacking α6β4 were unable to sustain *GPX4* mRNA expression (Fig. 7 A). That inability to up-regulate GPX4 was also seen at the protein level, and expression levels were rescued with exogenous β4 (Fig. 7 B).

Given that GPX4 buffers lipid peroxidation (Kriska and Girotti, 2005), we quantified lipid peroxidation in ECM-detached cells using the malondialdehyde (MDA) assay and observed that is was significantly greater in α6β4-depleted cells than it was in control cells (Fig. 7 C). In adherent conditions, loss of α6β4 increases lipid peroxidation compared with vector control; however, the loss of ECM contact significantly increases the burden of lipid peroxidation in those α6β4-depleted cells. Accordingly, glutathione peroxidase activity was elevated in detached, vector-controlled MCF10-A and SUM-159 cells compared with α6β4-depleted cells (Fig. 7 D).

To test whether the loss of GPX4 was responsible for the ferroptosis observed in α6β4-depleted cells upon ECM detachment, we expressed exogenous GPX4 in control and α6β4-depleted cells (Fig. 7 E). Exogenous GPX4 expression reduced cell death significantly in ECM-detached MCF10-A and SUM-159 cells lacking α6β4, but it had no effect on the viability of control cells (Fig. 7 F). Importantly, α6β4-depleted cells that expressed exogenous GPX4 were sensitive to erastin, consistent with the fact that system X_C^-, which is the target of erastin, functions upstream of GPX4 (Yang and Stockwell, 2016; Fig. 7 G).

Discussion

This study advances our knowledge of ferroptosis with respect to physiologic processes that trigger this form of cell death and mechanisms used by cells to resist it. As discussed recently, ferroptosis occurs when a "cell is sabotaged by its own ongoing normal cellular metabolic activity, such as the production of lipid hydroperoxides" and that it can be prevented if these normal activities are inhibited (Dixon, 2017). Our data substantiate that assessment and reveal that physiological (ECM detachment), as well as chemical (erastin), stimuli induce ferroptosis in epithelial and carcinoma cells. We also discovered a novel mechanism used by those cells to prevent such metabolic disruption that involves the α6β4 integrin. The fact that α6β4 expression is characteristic of epithelial and carcinoma cells suggests that those cells have acquired mechanisms to mitigate metabolic stresses that can trigger ferroptosis. Moreover, the ability of α6β4 to evade ferroptosis is not shared by other integrins expressed by those cells, including α6β1 and α3β1, based on our findings.

The key mechanism that we uncovered for the evasion of ferroptosis by α6β4 involves it ability to activate Src in stress

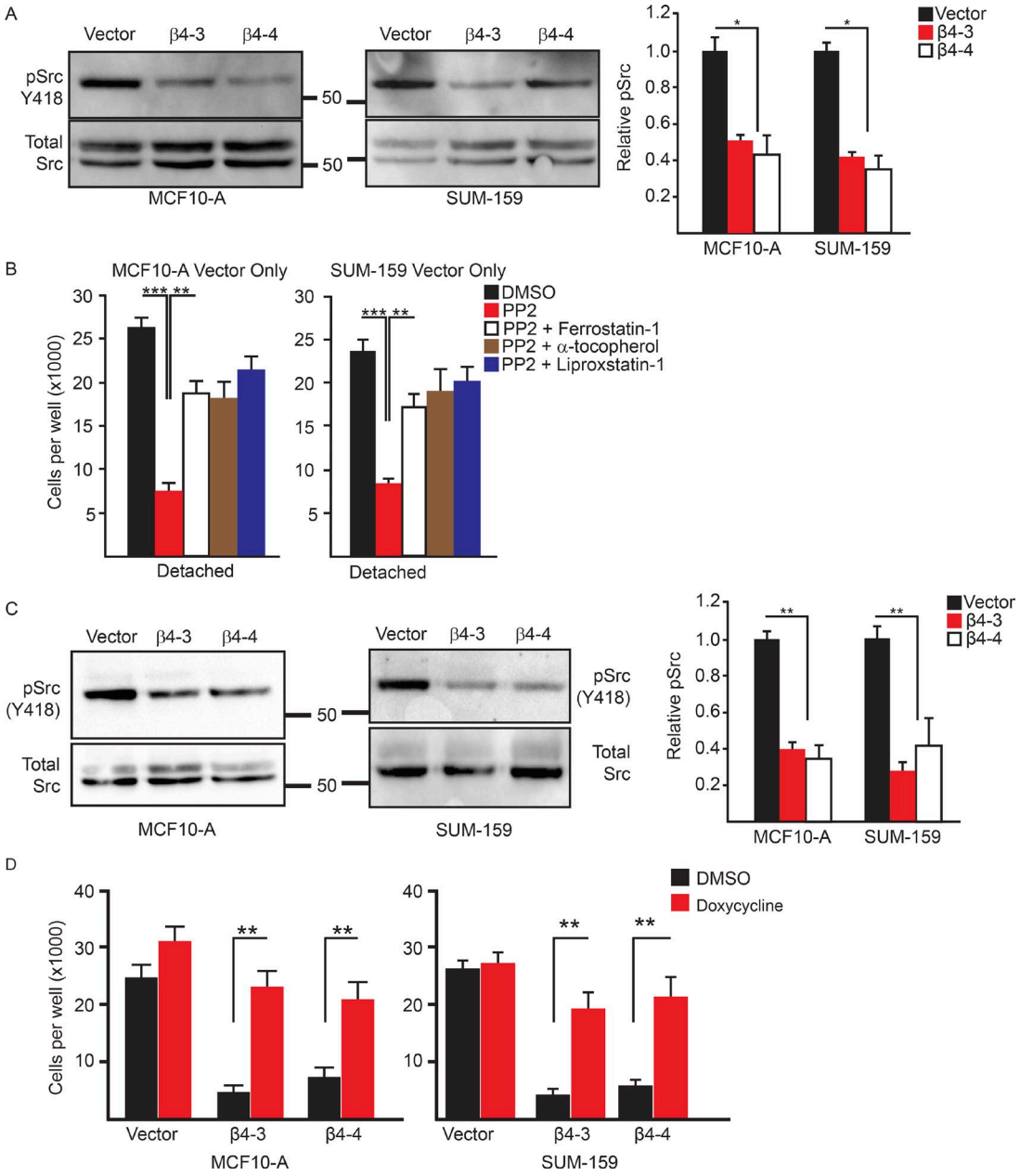

Figure 4. **The integrin α6β4 activates Src to inhibit ferroptosis.** (A) Vector control and β4-depleted cells were assessed for phosphorylated (Y418) Src by immunoblotting 3 h after ECM detachment. Relative phosphorylated Src was quantified by densitometry. (B) Vector control and β4-depleted cells were assessed for viability after 24 h of detachment in the presence of either DMSO, 10 µM PP2, PP2 and 2 µM ferrostatin-1, PP2 and 500 µM α-tocopherol, or PP2 and 2 µM liproxstatin-1. (C) Vector control and β4-depleted cells were assessed for phosphorylated (Y418) Src by immunoblotting after 3 h of incubation with 10 µM erastin. Relative phosphorylated Src was quantified by densitometry. (D) SUM-159 vector control and β4-depleted cells that expressed a doxycycline-inducible, constitutively active Src were incubated for 24 h with 2 µg/ml doxycycline and then assessed for viability after 24 h of detachment. All experiments were performed independently three times, and a representative experiment is shown. The bars in graphs represent means ± SD. *, P < 0.05; **, P < 0.01; ***, P < 0.005.

conditions and the consequent Src-mediated repression of ACSL4. ACSL4 generates a proferroptotic lipid composition in the plasma membrane, which is characterized by increased expression of long polyunsaturated ω6 fatty acids (Doll et al., 2017), and its repression nullifies the ferroptotic response (Doll et al., 2017). The α6β4-Src signaling axis is well established, and it has been implicated in the diverse functions associated with this integrin (Gagnoux-Palacios et al., 2003; Bertotti et al., 2006; Merdek et al., 2007; Dutta and Shaw, 2008; Yang et al., 2010; Sharma et al., 2012; Pavlova et al., 2013; Hoshino et al., 2015). The ability of Src to evade ferroptosis by repressing ACSL4 via the activation of STAT3, however, is novel and it provides one of the first examples of a major signaling mechanism that has the ability to resist the altered metabolic activity that can trigger this form of cell death. We demonstrate that α6β4-mediated Src activation contributes to ferroptosis resistance, but it is likely that other modes of Src activation result in such resistance, depending on the cellular context. Although not addressed directly, it is likely that α6β4-mediated Src activation in ECM-detached cells is independent of ligand

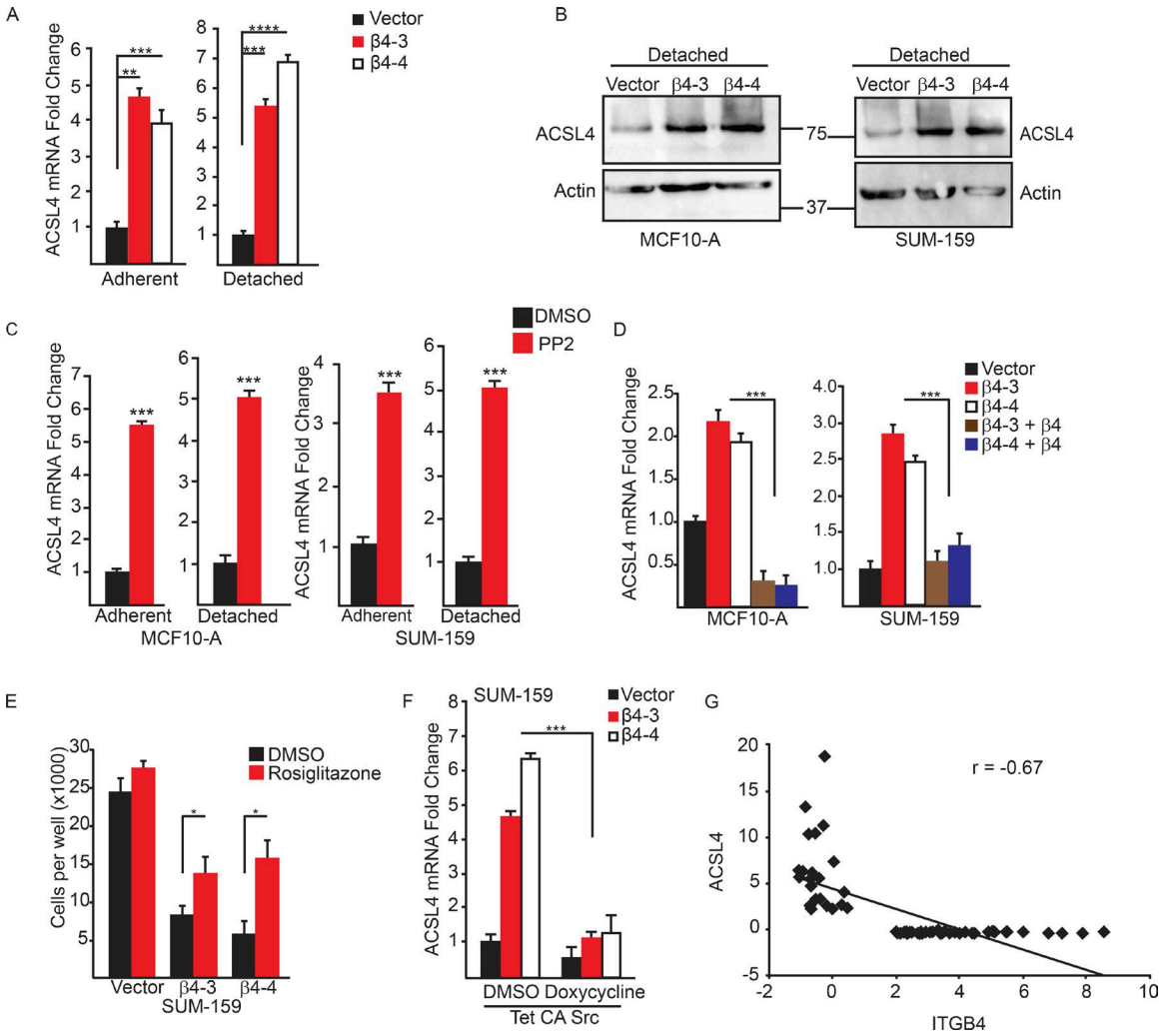

Figure 5. **The integrin α6β4 represses ACSL4 to inhibit ferroptosis.** Expression of ACSL4 was assessed by qPCR (A) and immunoblotting (B) in vector control and β4-depleted cells after 2 h of ECM detachment. (C) Expression of ACSL4 was quantified by qPCR in vector control MCF10-A or SUM-159 cells under either adherent or detached conditions after 2 h of treatment with DMSO or 10 µM PP2. (D) Expression of ACSL4 was quantified in adherent vector control, β4-depleted, and β4-rescued cells by qPCR. (E) Vector control and β4-depleted cells were assessed for viability after 24 h of detachment in the presence of either DMSO or the ACSL4 inhibitor 5 µM rosiglitazone. (F) SUM-159 vector control and β4-depleted adherent cells that expressed a doxycycline-inducible, constitutively active Src were incubated for 24 h with 2 µg/ml doxycycline, and the expression of ACSL4 was quantified by qPCR. (G) Expression of ITGB4 and ACSL4 was correlated using a published gene expression database (cBioportal) comprising 70 human breast tumors. The correlation coefficient (*r*) was calculated using Pearson's correlation. Experiments were performed independently three times, and a representative experiment is shown. The bars in graphs represent means ± SD. *, P < 0.05; **, P < 0.01; ***, P < 0.005.

(laminin), based on previous studies that addressed this issue (Pavlova et al., 2013).

Our finding that ECM detachment triggers ferroptosis is significant because little is known about physiologic or pathophysiologic mechanisms that are linked to this cell death process. Moreover, it is widely assumed that cells undergo apoptosis in response to ECM detachment (Meredith et al., 1993; Frisch and Francis, 1994), a phenomenon referred to as anoikis (Frisch and Francis, 1994). Although the discovery of anoikis has been a significant contribution to the field, the relationships among ECM detachment and cell death mechanisms are more complex and anoikis-independent pathways are also involved (Buchheit et al., 2014). There is also evidence that ECM detachment can increase intracellular ROS and cause ROS-dependent cell death (Schafer et al., 2009), although the mechanisms involved are not well understood (Buchheit et al., 2014). Our discovery that ECM detachment can trigger ferroptosis provides one mechanism for these results. As demonstrated here, ECM-detached cells are prone to both ferroptosis and apoptosis in the absence of α6β4. The apoptosis result is consistent with previous studies on this integrin (Bachelder et al., 1999; Zahir et al., 2003). Going forward, it will be important to determine the distinction between these two processes, particularly the point at which a decision is made by a cell to undergo either ferroptosis or apoptosis.

Although GPX4 is emerging as the critical gatekeeper of ferroptosis (Yang et al., 2014; Yang and Stockwell, 2016), biological mechanisms that regulate its expression or activity are poorly understood. In this direction, our findings substantiate the hypothesis that ferroptosis requires both GPX4 inhibition and ACSL4 activity. Adherent cells lacking α6β4 exhibit a significant increase in ACSL4 expression, but they are not prone to ferroptosis because GPX4 expression is sustained and it impedes lipid peroxidation. For that reason, these cells require an

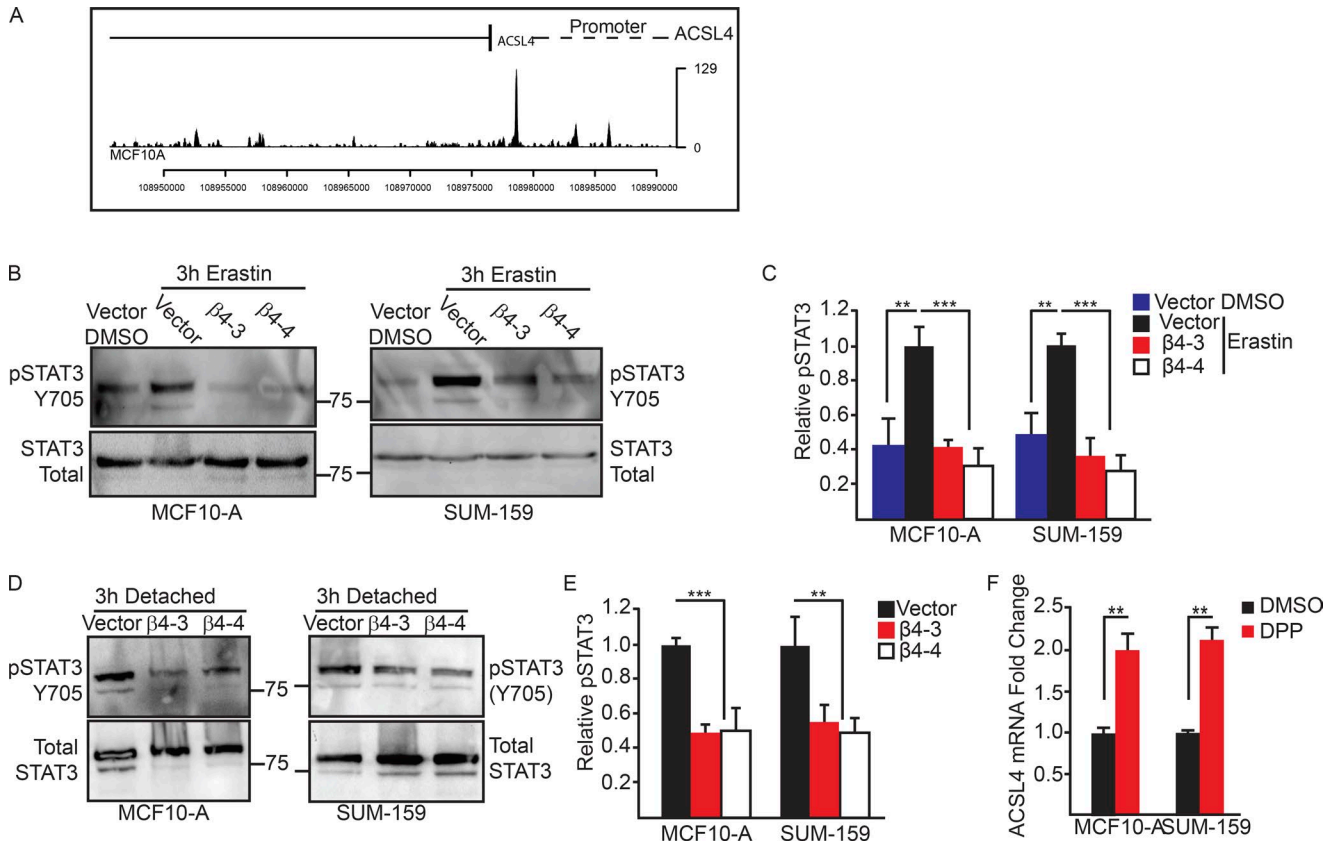

Figure 6. **STAT3 represses transcription of *ACSL4* downstream of the integrin α6β4.** (A) Analysis of MCF10-A cells using the ENCODE database showed binding of STAT3 to the promoter region. The phosphorylation of STAT3 was assessed by immunoblotting in vector control and β4-depleted MCF-10A cells after 3 h of detachment (B) or after incubation with erastin (D) and was also quantified by densitometry (C and E). (F) Expression of *ACSL4* was quantified by qPCR in vector control MCF10-A and SUM-159 adherent cells after 2 h of incubation with the STAT3 inhibitor DPP. Experiments were performed independently three times, and a representative experiment is shown. The bars in graphs represent means ± SD. **, P < 0.01; ***, P < 0.005.

exogenous inhibitor of GPX4, such as erastin, to undergo ferroptosis. In contrast, ECM detachment is sufficient to trigger ferroptosis in the absence of α6β4 because lipid peroxidation increases as a result of ACSL4 induction and diminished GPX4 expression. Our data indicate that α6β4 contributes to sustaining GPX4 expression in ECM-detached cells, but the mechanism appears to be distinct from α6β4-mediated repression of ACSL4 by Src because Src inhibition does not affect GPX4 expression (unpublished data).

The findings we present have potential implications for breast and other cancers. Although much is known about the mechanisms by which α6β4 contributes to epithelial biology and breast cancer, a cohesive mechanism has not emerged, and the possibility that this integrin protects tumor cells from excessive lipid peroxidation has not been considered. This mechanism is likely to be important for metastasis because this process involves detachment from ECM or the presence of the "foreign" ECM in a distant organ (Cheung and Ewald, 2016). Moreover, we detected a significant inverse correlation between α6β4 and ASCL4 in a large cohort of patients with breast cancer, and we demonstrated that the $\beta4^{low}$ population isolated from PDXs of human breast cancer is much more susceptible to ferroptosis induced by ECM detachment than is the $\beta4^{high}$ population. This latter observation is of particular interest because some chemotherapeutic drugs, as well as more novel therapies, such as the use of nanoparticles to deliver tumor-targeting peptides, function by inducing ferroptosis (Yang et al., 2014; Kim et al., 2016). Our data suggest that tumor cells with high α6β4 expression could be resistant to such therapies.

Materials and methods

Cell lines and reagents

MCF10-A cells were obtained from the Barbara Ann Karmanos Cancer Institute, and SUM-159 cells were provided by S. Ethier (Medical College of South Carolina, Charleston, SC). Hs578T cells were provided by D. Kim (University of Massachusetts Medical School, Worcester, MA). The pCMV-β4 plasmid was provided by L. Shaw (University of Massachusetts Medical School, Worcester, MA). A Tet-CA-Src-GFP construct was purchased from Addgene (plasmid 83469). All cells were checked quarterly for mycoplasma.

The following antibodies were used: GPX4 (Abcam), actin (Sigma-Aldrich), integrin β4 (505 [Rabinovitz et al., 1999] and 439-9b [Abcam]), α6 (GoH3; MilliporeSigma), and integrin β1 (BD), phospho-Src Y418 (R&D Systems), total Src (Santa Cruz Biotechnology, Inc.), ACSL4 (Santa Cruz Biotechnology, Inc.), phospho-STAT3 Y705 (Cell Signaling Technology), and total STAT3 (Cell Signaling Technology). Other reagents used were: Z-VAD-FMK (SelleckChem), erastin (Sigma-Aldrich), ferrostatin-1 (Sigma-Aldrich), liproxstatin-1 (Sigma-Aldrich), DFO mesylate salt (Sigma-Aldrich), α-tocopherol (Sigma-Aldrich), trolox (Sigma-Aldrich), DPP (Sigma-Aldrich), and rosiglitazone (Tocris Bioscience).

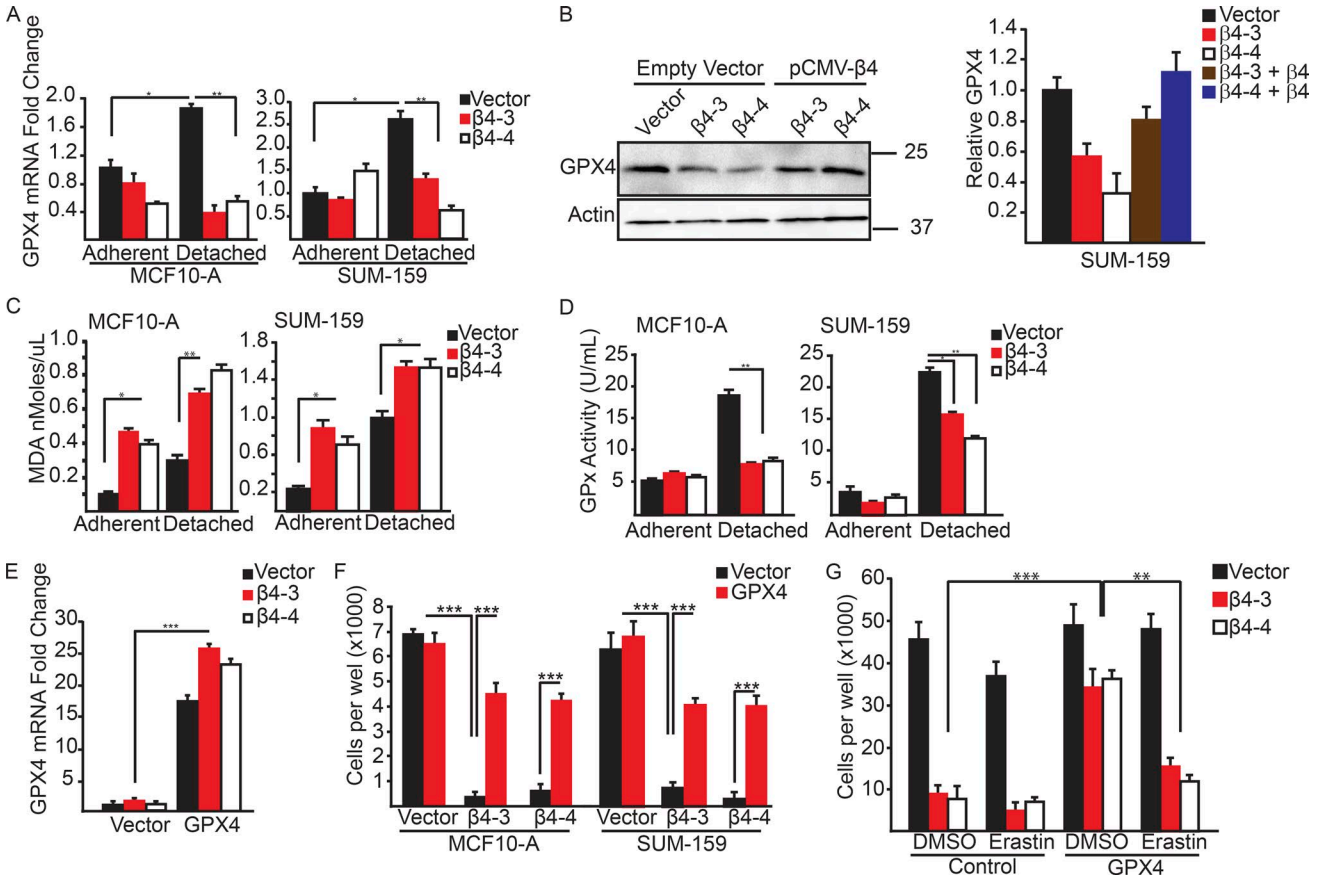

Figure 7. **Matrix-deprived cells exhibit increased lipid peroxidation and an inability to sustain GPX4 expression in the absence of the α6β4-integrin.** (A) GPX4 mRNA expression was quantified by qPCR in control and β4-depleted MCF-10A and SUM-159 cells under adherent or 2-h matrix-deprived conditions. (B) Expression of GPX4 was assessed by immunoblotting in vector control, β4-depleted, and β4-rescued cells after 2 h of detachment. Relative densitometry values are shown. (C) Lipid peroxidation was quantified using the MDA assay in control and β4-depleted, MCF-10A and SUM-159 cells under adherent or 4-h matrix-deprived conditions. (D) GPX enzyme activity was assayed in control and β4-depleted, MCF-10A and SUM-159 cells under adherent or 4-h matrix-deprived conditions. (E) Control and β4-depleted SUM-159 cells were transfected with either a vector control or a GPX4 expression vector. GPX4 mRNA expression was quantified by qPCR. (F) Control and β4-depleted MCF10-A and SUM-159 cells that had been transfected with either a vector control or a GPX4 expression vector were detached for 24 h, and the number of viable cells was quantified. (G) Control and β4-depleted cells that had been transfected with either a vector control or a GPX4 expression vector were detached for 24 h with in the presence of either DMSO or 10 μM erastin, and the number of viable cells was quantified. Experiments were performed independently three times and a representative experiment is shown. The bars in graphs represent means ± SD. *, P < 0.05; **, P < 0.01; ***, P < 0.005.

RNA interference

Lentiviruses containing ITGA3 shRNAs (clone ID TRCN0000057713 or TRCN0000057714; GE Healthcare) or a GFP control (RHS4459) were generated, titrated according to the manufacturer's instructions, and used to transiently infect MCF10-A and SUM-159 vector control and β4-depleted cells, following standard protocols.

PDX tumors

PDX models of triple-negative breast cancer were obtained from the Dana-Farber Cancer Institute and propagated in NSG mice. Tumors were harvested and digested using collagenase at 37°C. Once digested, the cells were filtered using a cell strainer (40 μm), washed twice with PBS, and plated in DMEM/F12 (containing 10% FBS). The next day, cells were stained using a β4 antibody for 1 h and analyzed by flow cytometry. The highest and lowest quartiles of cells expressing β4 were collected and plated immediately for experimentation.

Colony formation assay

MCF10-A and SUM-159 vector control or β4-depleted cells (5×10^2) were plated on 60-mm dishes. 24 h after plating, cells were incubated in medium containing erastin (10 μM), erastin and ferrostatin-1 (2 μM), or DMSO control. Media were changed daily with continued exposure. 10 d after the first treatment, plates were washed in PBS, fixed in 4% paraformaldehyde, and stained in crystal violet. Plates were washed clean of excess dye and colonies >50 cells were counted. For some experiments, the crystal violet–stained cells were solubilized with DMSO, and absorbance was read at 590 nm.

Matrix-detachment assays

24-well plates were coated with poly 2-hydroxyethyl methacrylate (polyHEMA; 30 mg/ml; Sigma-Aldrich) and dried overnight. Trypsinized cells were plated (2.5×10^4 per well) in serum-free medium with the reagents indicated in the figure legends for the times noted. Cells were counted with a hemocytometer using trypan blue exclusion. Total cell number was calculated by multiplying the mean of cells per square by the dilution factor and chamber volume.

Biochemical experiments

For immunoblotting, cells were extracted using radioimmunoprecipitation assay buffer containing protease inhibitors (Boston BioProducts). Extracts were separated by SDS-PAGE and immunoblotted using the antibodies specified in the figure legends. Immunoprecipitation was

performed on precleared lysates by incubation with the primary antibody and, subsequently, protein G sepharose beads (Sigma-Aldrich). Immune complexes were dissociated, and proteins were separated by SDS-PAGE and immunoblotted as described in the figure legends. For qPCR, RNA was isolated from cells with NucleoSpin Gel and the PCR Clean-Up kit (Macherey-Nagel), and cDNAs were produced using the All-In-One cDNA Synthesis SuperMix (BioScript Solutions). qPCR was performed using a SYBR Green master mix (biotool.com). Sequences for primers used are provided in Table S1. The two-tailed Student *t* test was used to assess statistical significance.

To assess cytotoxicity, the LDH assay (Thermo Fisher Scientific) was used, according to the manufacturer's specifications. In brief, 5,000 cells were cultured in 96-well adherent or polyHEMA-coated plates in serum-free media for 4 h in DMSO, erastin (10 µM), or ferrostatin-1 (2 µM), as indicated. Medium from each well was reacted to form red formazan. Absorbance was read at 490 and 680 nm, and the LDH per well was calculated.

To assay lipid peroxidation, the MDA lipid peroxidation microplate assay (Sigma-Aldrich) was used according to manufacturer's specifications. In brief, cells (10^6) were cultured in serum-free medium on polyHEMA-coated plates for 4 h. Cells were collected, lysed, and reacted with thiobarbituric acid. Fluorescence was read at 532 (excitation) and 590 (emission). Lipid peroxidation levels were normalized to protein concentration. Glutathione peroxidase activity assay (BioVision) was performed according to the manufacturer's specifications. In brief, cells (10^6) were trypsinized and cultured in serum-free medium on polyHEMA-coated plates for 4 h. Cells were lysed and challenged with cumene hydroperoxide to assess the activity of glutathione peroxides. Plates were read at 340 nm 5 min after challenge. Glutathione peroxidase activity was normalized to protein concentration.

Molecular biology experiments

For CRISPR-mediated deletion of the β4 integrin subunit, guide RNAs targeting exon 1 of the β4 sequence were selected using two websites, CRISPR Design (http://crispr.mit.edu) and CRISPRdirect (https://crispr.dbcls.jp). Four guide RNAs were tested, and the two most efficient knockouts were selected and used to control for potential off-target effects. Cells were subcloned by FACS and screened for loss of protein expression by immunoblot. To rescue the β4 deletion, the protospacer-adjacent motif (PAM) sequences targeted by the guide RNAs were mutated using the New England Biolabs, Inc., Q5 site-directed mutagenesis kit in pcDNA3.1-Myc-β4 (16039; Addgene). Mutagenesis primers were designed using the New England BioLabs, Inc., BaseChanger tool. Silent mutations were used to prevent changes in the amino acid sequence (Table S1). To express constitutively active Src, MCF10-A and SUM-159 vector control or β4-depleted cells were incubated with lentiviral-packaged Tet-CA-Src-GFP for 24 h before selection with 2 µg/ml puromycin for 7 d. Src expression was induced by 24-h incubation with 2 µg/ml doxycycline. To express GPX4, a plasmid construct for GPX4 was purchased from OriGene (RC208065). Cells were transfected with 10 µg DNA using Lipofectamine 2000 (Thermo Fisher Scientific) and incubated for 48 h before use.

ENCODE database analysis

The signal of the STAT3 chromatin immunoprecipitation sequencing on the human MCF10A cell line (a stably expressed Er–Src fusion protein treated with 0.01% ethanol) was downloaded from the ENCODE project (https://www.encodeproject.org/experiments/ENCSR000DOZ/; National Human Genome Research Institute). The track was plotted with the Bioconductor trackViewer (version 1.12.0) package.

Statistical analysis

The bars in graphs represent means ± SD. All experiments were repeated at least three times. The p-value was calculated using Student's *t* test and a p-value <0.05 was considered significant.

Online supplemental material

Table S1 lists the primers used for qPCR and mutagenesis analyses.

Acknowledgments

We thank Joan Brugge for helpful discussions. We also thank Jianhong Ou and Julie Zhu of our departmental bioinformatics core for assistance with the ENCODE database analysis and Huayan Sun for creation of the β4 CRISPR plasmids.

This work was supported by U.S. Department of Defense grant W81XWH-17-1-0009 and National Institutes of Health grant CA 203439. C.W. Brown was supported by American Cancer Society grant 130451-PF-17-105-01-CSM.

The authors declare no competing financial interests.

Author contributions: C.W. Brown and A.M. Mercurio conceived the study, designed the experiments, oversaw the project, and wrote the manuscript. C.W. Brown executed and interpreted the experiments. J.J. Amante provided technical assistance and prepared the final figures. H.L. Goel provided insightful input on the study and critical analysis of the data and contributed to writing the manuscript.

Submitted: 10 January 2017
Revised: 8 June 2017
Accepted: 22 August 2017

References

Askari, B., J.E. Kanter, A.M. Sherrid, D.L. Golej, A.T. Bender, J. Liu, W.A. Hsueh, J.A. Beavo, R.A. Coleman, and K.E. Bornfeldt. 2007. Rosiglitazone inhibits acyl-CoA synthetase activity and fatty acid partitioning to diacylglycerol and triacylglycerol via a peroxisome proliferator-activated receptor-gamma-independent mechanism in human arterial smooth muscle cells and macrophages. *Diabetes.* 56:1143–1152. https://doi.org/10.2337/db06-0267

Bachelder, R.E., M.J. Ribick, A. Marchetti, R. Falcioni, S. Soddu, K.R. Davis, and A.M. Mercurio. 1999. p53 inhibits α6β4 integrin survival signaling by promoting the caspase 3-dependent cleavage of AKT/PKB. *J. Cell Biol.* 147:1063–1072. https://doi.org/10.1083/jcb.147.5.1063

Bertotti, A., P.M. Comoglio, and L. Trusolino. 2006. β4 integrin activates a Shp2-Src signaling pathway that sustains HGF-induced anchorage-independent growth. *J. Cell Biol.* 175:993–1003. https://doi.org/10.1083/jcb.200605114

Buchheit, C.L., K.J. Weigel, and Z.T. Schafer. 2014. Cancer cell survival during detachment from the ECM: multiple barriers to tumour progression. *Nat. Rev. Cancer.* 14:632–641. https://doi.org/10.1038/nrc3789

Cheung, K.J., and A.J. Ewald. 2016. A collective route to metastasis: Seeding by tumor cell clusters. *Science.* 352:167–169. https://doi.org/10.1126/science.aaf6546

DiPersio, C.M., K.M. Hodivala-Dilke, R. Jaenisch, J.A. Kreidberg, and R.O. Hynes. 1997. α3β1 Integrin is required for normal development of the epidermal basement membrane. *J. Cell Biol.* 137:729–742. https://doi.org/10.1083/jcb.137.3.729

Dixon, S.J. 2017. Ferroptosis: bug or feature? *Immunol. Rev.* 277:150–157. https://doi.org/10.1111/imr.12533

Dixon, S.J., K.M. Lemberg, M.R. Lamprecht, R. Skouta, E.M. Zaitsev, C.E. Gleason, D.N. Patel, A.J. Bauer, A.M. Cantley, W.S. Yang, et al. 2012. Ferroptosis: an iron-dependent form of nonapoptotic cell death. *Cell.* 149:1060–1072. https://doi.org/10.1016/j.cell.2012.03.042

Doll, S., B. Proneth, Y.Y. Tyurina, E. Panzilius, S. Kobayashi, I. Ingold, M. Irmler, J. Beckers, M. Aichler, A. Walch, et al. 2017. ACSL4 dictates ferroptosis sensitivity by shaping cellular lipid composition. *Nat. Chem. Biol.* 13:91–98. https://doi.org/10.1038/nchembio.2239

Dutta, U., and L.M. Shaw. 2008. A key tyrosine (Y1494) in the β4 integrin regulates multiple signaling pathways important for tumor development

and progression. *Cancer Res.* 68:8779–8787. https://doi.org/10.1158/0008-5472.CAN-08-2125

Friedmann Angeli, J.P., M. Schneider, B. Proneth, Y.Y. Tyurina, V.A. Tyurin, V.J. Hammond, N. Herbach, M. Aichler, A. Walch, E. Eggenhofer, et al. 2014. Inactivation of the ferroptosis regulator Gpx4 triggers acute renal failure in mice. *Nat. Cell Biol.* 16:1180–1191. https://doi.org/10.1038/ncb3064

Frisch, S.M., and H. Francis. 1994. Disruption of epithelial cell-matrix interactions induces apoptosis. *J. Cell Biol.* 124:619–626. https://doi.org/10.1083/jcb.124.4.619

Gagnoux-Palacios, L., M. Dans, W. van't Hof, A. Mariotti, A. Pepe, G. Meneguzzi, M.D. Resh, and F.G. Giancotti. 2003. Compartmentalization of integrin α6β4 signaling in lipid rafts. *J. Cell Biol.* 162:1189–1196. https://doi.org/10.1083/jcb.200305006

Giancotti, F.G. 2007. Targeting integrin β4 for cancer and anti-angiogenic therapy. *Trends Pharmacol. Sci.* 28:506–511. https://doi.org/10.1016/j.tips.2007.08.004

Guo, W., Y. Pylayeva, A. Pepe, T. Yoshioka, W.J. Muller, G. Inghirami, and F.G. Giancotti. 2006. β 4 integrin amplifies ErbB2 signaling to promote mammary tumorigenesis. *Cell.* 126:489–502. https://doi.org/10.1016/j.cell.2006.05.047

Hanahan, D., and R.A. Weinberg. 2011. Hallmarks of cancer: the next generation. *Cell.* 144:646–674. https://doi.org/10.1016/j.cell.2011.02.013

Hoshino, A., B. Costa-Silva, T.L. Shen, G. Rodrigues, A. Hashimoto, M. Tesic Mark, H. Molina, S. Kohsaka, A. Di Giannatale, S. Ceder, et al. 2015. Tumour exosome integrins determine organotropic metastasis. *Nature.* 527:329–335. https://doi.org/10.1038/nature15756

Jiang, L., N. Kon, T. Li, S.J. Wang, T. Su, H. Hibshoosh, R. Baer, and W. Gu. 2015. Ferroptosis as a p53-mediated activity during tumour suppression. *Nature.* 520:57–62. https://doi.org/10.1038/nature14344

Kim, S.E., L. Zhang, K. Ma, M. Riegman, F. Chen, I. Ingold, M. Conrad, M.Z. Turker, M. Gao, X. Jiang, et al. 2016. Ultrasmall nanoparticles induce ferroptosis in nutrient-deprived cancer cells and suppress tumour growth. *Nat. Nanotechnol.* 11:977–985. https://doi.org/10.1038/nnano.2016.164

Kriska, T., and A.W. Girotti. 2005. A thin layer chromatographic method for determining the enzymatic activity of peroxidases catalyzing the two-electron reduction of lipid hydroperoxides. *J. Chromatogr. B Analyt. Technol. Biomed. Life Sci.* 827:58–64. https://doi.org/10.1016/j.jchromb.2005.03.045

Lipscomb, E.A., and A.M. Mercurio. 2005. Mobilization and activation of a signaling competent alpha6beta4integrin underlies its contribution to carcinoma progression. *Cancer Metastasis Rev.* 24:413–423. https://doi.org/10.1007/s10555-005-5133-4

Merdek, K.D., X. Yang, C.A. Taglienti, L.M. Shaw, and A.M. Mercurio. 2007. Intrinsic signaling functions of the β4 integrin intracellular domain. *J. Biol. Chem.* 282:30322–30330. https://doi.org/10.1074/jbc.M703156200

Meredith, J.E. Jr., B. Fazeli, and M.A. Schwartz. 1993. The extracellular matrix as a cell survival factor. *Mol. Biol. Cell.* 4:953–961. https://doi.org/10.1091/mbc.4.9.953

Niu, G., K.L. Wright, Y. Ma, G.M. Wright, M. Huang, R. Irby, J. Briggs, J. Karras, W.D. Cress, D. Pardoll, et al. 2005. Role of Stat3 in regulating p53 expression and function. *Mol. Cell. Biol.* 25:7432–7440. https://doi.org/10.1128/MCB.25.17.7432-7440.2005

Pavlova, N.N., C. Pallasch, A.E. Elia, C.J. Braun, T.F. Westbrook, M. Hemann, and S.J. Elledge. 2013. A role for PVRL4-driven cell-cell interactions in tumorigenesis. *eLife.* 2:e00358. https://doi.org/10.7554/eLife.00358

Rabinovitz, I., A. Toker, and A.M. Mercurio. 1999. Protein kinase C-dependent mobilization of the α6β4 integrin from hemidesmosomes and its association with actin-rich cell protrusions drive the chemotactic migration of carcinoma cells. *J. Cell Biol.* 146:1147–1160. https://doi.org/10.1083/jcb.146.5.1147

Roveri, A., M. Maiorino, C. Nisii, and F. Ursini. 1994. Purification and characterization of phospholipid hydroperoxide glutathione peroxidase from rat testis mitochondrial membranes. *Biochim. Biophys. Acta.* 1208:211–221. https://doi.org/10.1016/0167-4838(94)90106-6

Safa, A.R. 2016. Resistance to Cell Death and Its Modulation in Cancer Stem Cells. *Crit. Rev. Oncog.* 21:203–219. https://doi.org/10.1615/CritRevOncog.2016016976

Schafer, Z.T., A.R. Grassian, L. Song, Z. Jiang, Z. Gerhart-Hines, H.Y. Irie, S. Gao, P. Puigserver, and J.S. Brugge. 2009. Antioxidant and oncogene rescue of metabolic defects caused by loss of matrix attachment. *Nature.* 461:109–113. https://doi.org/10.1038/nature08268

Seiler, A., M. Schneider, H. Förster, S. Roth, E.K. Wirth, C. Culmsee, N. Plesnila, E. Kremmer, O. Rådmark, W. Wurst, et al. 2008. Glutathione peroxidase 4 senses and translates oxidative stress into 12/15-lipoxygenase dependent- and AIF-mediated cell death. *Cell Metab.* 8:237–248. https://doi.org/10.1016/j.cmet.2008.07.005

Sharma, C., I. Rabinovitz, and M.E. Hemler. 2012. Palmitoylation by DHHC3 is critical for the function, expression, and stability of integrin α6β4. *Cell. Mol. Life Sci.* 69:2233–2244. https://doi.org/10.1007/s00018-012-0924-6

Thomas, J.P., P.G. Geiger, M. Maiorino, F. Ursini, and A.W. Girotti. 1990. Enzymatic reduction of phospholipid and cholesterol hydroperoxides in artificial bilayers and lipoproteins. *Biochim. Biophys. Acta.* 1045:252–260. https://doi.org/10.1016/0005-2760(90)90128-K

Yang, W.S., and B.R. Stockwell. 2016. Ferroptosis: Death by Lipid Peroxidation. *Trends Cell Biol.* 26:165–176. https://doi.org/10.1016/j.tcb.2015.10.014

Yang, W.S., R. SriRamaratnam, M.E. Welsch, K. Shimada, R. Skouta, V.S. Viswanathan, J.H. Cheah, P.A. Clemons, A.F. Shamji, C.B. Clish, et al. 2014. Regulation of ferroptotic cancer cell death by GPX4. *Cell.* 156:317–331. https://doi.org/10.1016/j.cell.2013.12.010

Yang, W.S., K.J. Kim, M.M. Gaschler, M. Patel, M.S. Shchepinov, and B.R. Stockwell. 2016. Peroxidation of polyunsaturated fatty acids by lipoxygenases drives ferroptosis. *Proc. Natl. Acad. Sci. USA.* 113:E4966–E4975. https://doi.org/10.1073/pnas.1603244113

Yang, X., U. Dutta, and L.M. Shaw. 2010. SHP2 mediates the localized activation of Fyn downstream of the α6β4 integrin to promote carcinoma invasion. *Mol. Cell. Biol.* 30:5306–5317. https://doi.org/10.1128/MCB.00326-10

Yu, C.L., D.J. Meyer, G.S. Campbell, A.C. Larner, C. Carter-Su, J. Schwartz, and R. Jove. 1995. Enhanced DNA-binding activity of a Stat3-related protein in cells transformed by the Src oncoprotein. *Science.* 269:81–83. https://doi.org/10.1126/science.7541555

Zahir, N., J.N. Lakins, A. Russell, W. Ming, C. Chatterjee, G.I. Rozenberg, M.P. Marinkovich, and V.M. Weaver. 2003. Autocrine laminin-5 ligates α6β4 integrin and activates RAC and NFκB to mediate anchorage-independent survival of mammary tumors. *J. Cell Biol.* 163:1397–1407. https://doi.org/10.1083/jcb.200302023